Advances in Concrete Construction, *Vol. 19*, *No. 6* (*2025*) *349-362*
https://doi.org/10.12989/acc.2025.19.6.349

Optimal surface for corner combined footings assuming that the ground contact area works partially in compression considering that the maximum pressure is located at the corner of the footing: Part 1

Arnulfo Luévanos-Rojas*

Institute of Multidisciplinary Researches, *Autonomous University of Coahuila*,
Blvd. Revolución No, *151 Ote*, *CP 27000*, *Torreón*, *Coahuila*, *México*

(*Received October 9*, *2023*, *Revised April 20*, *2025*, *Accepted April 29*, *2025*)

Abstract. This paper presents the optimal surface for corner combined footings assuming that the contact area with the soil works partially in compression (one part of the contact surface of the footing is subjected to compression and the other part is not subjected to compression or tension). The methodology is developed by integration to obtain the resultant force and resultant moments on the X and Y axes acting on the footing due to soil pressure. The three types that can occur depending on the location of the maximum pressure are: 1) Corner of the footing; 2) At one end and on the outer side of the footing; 3) At one end and on the inner side of the footing. In this work, the simplified equations are shown when the maximum pressure is located in corner of the footing. Some engineers obtain the contact area of the footing by the trial and error method. Other authors present the minimum area for a corner combined footing taking into account that the contact area with the soil works completely in compression. Numerical examples are shown to obtain the minimum area of the footings and the results are compared with the current model. The new model shows a smaller soil contact area in some cases than the current model.

Keywords: contact area works partially to compression; corner combined footings; linear pressure distribution of the soil; optimal surface; resultant force; resultant moments

1. Introduction

Footing or foundation is the structural member (sub-structure) that transfers the loads of the superstructure to the soil. Footings are used in various types of construction in structural engineering, such as buildings and bridges.

The main purpose of geotechnical and structural engineering is to obtain the smallest area and the dimensions of the footing to support the imposed loads by the superstructure.

The total contact pressure depends on the position of the resultant force "R", the base of the footing can be completely compressed or a fraction of it can be without compression and without tension (zero pressure). The area that works under compression is called the active compression zone, and the zero pressure condition defined by the neutral axis "NA".

The mathematical models to obtain the contact area on the soil have been developed for square (Luévanos-Rojas 2012a), rectangular (Luévanos-Rojas 2013) and circular (Luévanos-Rojas 2012b) isolated footings subjected to biaxial bending. Also, models for combined footings have been proposed to obtain the contact surface on the soil subjected to biaxial bending in each column of rectangular shape (Luévanos-Rojas 2016), trapezoidal (Luévanos-Rojas 2015a), L-shaped (López-Chavarría *et al*. 2017), strap (Aguilera-Mancilla *et al*. 2019) and T-shaped (Luévanos-Rojas *et al*. 2018a). These papers take into account the entire contact area working under compression.

The studies on the bearing capacity of shallow footings subjected to uniaxial bending, taking into account the area of the footing that works partially under compression are: Peck *et al*. (1974) proposed an iterative method for arbitrarily shaped foundations. Teng (1979) presented graphs and equations for rectangular footings. Young and Budynas (2002) proposed tables and a general graphical method based on trial and error for rectangular footings. Highter and Anders (1985) developed design aids for circular and rectangular footings based on the concept of reduced effective area.

The investigations on the bearing capacity of shallow footings subjected to biaxial bending are: Irles-Más and Irles-Más (1992) proposed an analytical solution to determine the pressure generated by the soil on the rectangular footings. Özmen (2011) proposed a successive approximations process to calculate the pressures below the rectangular footings. Rodriguez-Gutierrez and Aristizabal-Ochoa (2013a) presented a simplified method to estimate the biaxial moment and axial load capacities of a rigid footing of arbitrary or regular shape that rests on the soil. Rodriguez-Gutierrez and Aristizabal-Ochoa (2013b) proposed several design aids (nomograms) for rectangular and trapezoidal rigid footings for three different types of pressure distribution for the types of uniform, linear, and parabolic. Bashir *et al*. (2013) used the 3D finite element

*Corresponding author, Ph.D., Professor,
E-mail: arnulfol_2007@hotmail.com

http://www.techno-press.org/?journal=acc&subpage=7
ISSN: 2287-5301 (Print), 2287-531X (Online)

program to predict the moment anchorage capacity and experimentally verified. Lee *et al*. (2015) developed a 3D numerical method to obtain the settlement behavior of flexible mat foundations under vertical loads, taking into account the coupled soil springs. Kaur and Kumar (2016) used a statistical model for nonlinear regression analysis based on experimental data to predict the vertical settlement, horizontal deformation and tilt of a square footing subjected to any load supported on reinforced sand. Bezmalinovic Colleoni (2016) developed analytical equations to determine the linear pressure distribution of soil under the rigid rectangular footings. Aydogdu (2016) presented an iterative method to calculate the pressure below rectangular footings. Girgin (2017) obtained the rotational spring constants for rigid rectangular isolated footings resting on soil without tension and compression. Turedi *et al*. (2019) investigated the load-settlement and vertical stress of the ring footings supported on the loose sand bed through numerical analysis and laboratory tests. Al-Gahtani and Adekunle (2019) proposed an accurate and efficient, simple formulation to calculate the soil stresses due to arbitrarily distributed pressures over an arbitrarily shaped surface. Galvis and Smith-Pardo (2020) developed design aids to obtain the axial load and biaxial moment capacity for rectangular and circular shallow footings. Rawat *et al*. (2020) presented a critical evaluation and proposed a simplified analysis methodology for rectangular isolated footings. Lu and Aboutaha (2021) introduced three strengthening systems for isolated footings: BFRP wrapping system, CFRP wrapping system, and steel jacketing system. Lezgy-Nazargah *et al*. (2022) analyzed shallow ground-supported footings using a mixed-field plate finite element model. Gör (2022) investigated the efficiency of two metaheuristic-based models; the black hole algorithm and multi-verse optimizer are synthesized with an artificial neural network to build the proposed hybrid models. Mansour *et al*. (2022) investigated experimentally and numerically the punching behavior of reinforced concrete isolated footings. Himeur *et al*. (2022) studied the coupled effect of variable Winkler–Pasternak foundations on the bending behavior of plates exposed to several types of loading. Dai *et al*. (2023) applied the six neural network-based solutions to the bearing capacity of shallow footing on double-layer soils. Belabed *et al*. (2024) examined the bending and buckling behaviors of functionally graded carbon nanotube-reinforced composite beams resting on Winkler-Pasternak elastic foundations by the finite element model.

Several researchers presented complete optimal designs for foundations such as: Khajehzadeh *et al*. (2014) for the foundations using the global-local gravitational search algorithm, Luévanos-Rojas (2014) for circular isolated footings, Luévanos-Rojas (2015b) for trapezoidal combined footings of edge, Luévanos-Rojas *et al*. (2017) for rectangular isolated footings, Velázquez-Santillán *et al*. (2018) for rectangular combined footings, Luévanos-Rojas *et al*. (2018b) for T-shaped combined footings, López-Chavarría *et al*. (2019) for circular isolated footings, Yáñez-Palafox *et al*. (2019) for strap combined footings, Luévanos-Rojas (2023a) for the optimal design of trapezoidal combined footings, Luévanos-Rojas *et al*. (2024a) for the optimal design of strap combined footings, Luévanos-Rojas *et al*. (2024b) for the optimal design of circular isolated footings with eccentric column. These papers take into account the entire contact area working under compression.

The papers that present the minimum contact area with the ground that work partially in compression are: Soto-García *et al*. (2022) for circular isolated footings; Vela-Moreno *et al*. (2022) for rectangular isolated footings; Montes-Paramo *et al*. (2023) for rectangular combined footings; Luévanos-Rojas (2023b) for the complete design of rectangular isolated footings; Luévanos-Soto (2024a) for circular isolated footings with eccentric column; Luévanos-Soto (2024b) for the complete design of circular isolated footings with eccentric column.

This research shows a mathematical model to obtain the minimum area for the corner combined footings subjected to biaxial bending at each column that considers the contact surface with the soil working partially under compression, i.e., a part of the contact surface of the footing is subject to compression and the other there is no pressure (pressure zero). The three types that can occur depending on the location of the maximum pressure are: 1) Corner of the footing; 2) At one end and on the outer side of the footing; 3) At one end and on the inner side of the footing. In this work, the simplified equations are shown for type 1. The optimal model is formulated from a mathematical approach based on a minimum area, and it is developed by integration to obtain the resultant force "R", resultant moment around the X axis "M_{xT}" and resultant moment around the Y axis "M_{yT}". The known or constant parameters (independent variables) are: $\sigma_{\max}$, P_1, P_2, P_3, M_{x1}, M_{x2}, M_{x3}, M_{y1}, M_{y2} and M_{y3}. The unknown or decision variables (dependent variables) are: $A_{\min}$, a_1, a_2, a_3, b, h, h_1, x_1, x_2, x_d, y_1, y_2, y_s, M_{xT} and M_{yT}. Some designers obtain the footing contact area by the trial and error method and others obtain the minimum area for a corner combined footing, but take into account that the soil contact area works entirely under compression. Numerical examples are presented to obtain the footing minimum area and compared with the current model to observe the differences.

2. Methodology

The loads and moments are obtained from a structural analysis, where the analysis of the structural framework is developed by any of the known methods (Stiffness Method, Slope-Deflection Method and Hardy Cross Method) that include dead, live, wind, and earthquake.

The rigid footing deforms in a planar manner, i.e., the distribution of soil pressure under the footing is considered to be linear.

The biaxial bending equation is not valid, when the resultant force R is located outside of the central nucleus, a well-known and delimited area, indicating an uncompressed zone.

Fig. 1 shows the geometric properties of a corner combined footing.

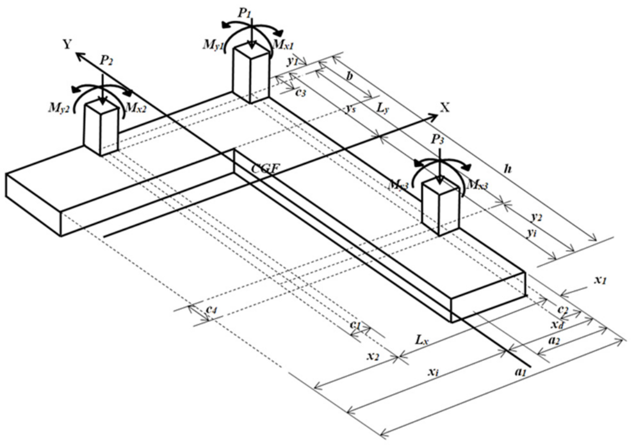

Fig. 1 Geometric properties for a corner combined footing

The geometric properties of the ˥-shaped section are

$$A = (a_1 - a_2)b + a_2 h \tag{1}$$

$$y_s = \frac{(a_1 - a_2)b^2 + a_2 h^2}{2[(a_1 - a_2)b + a_2 h]} \tag{2}$$

$$y_i = \frac{(2h - b)(a_1 - a_2)b + a_2 h^2}{2[(a_1 - a_2)b + a_2 h]} \tag{3}$$

$$x_d = \frac{{a_1}^2 b + {a_2}^2 (h - b)}{2[(a_1 - a_2)b + a_2 h]} \tag{4}$$

$$x_i = \frac{{a_1}^2 b + a_2(2a_1 - a_2)(h - b)}{2[(a_1 - a_2)b + a_2 h]} \tag{5}$$

$$I_x = \frac{(a_1 - a_2)b^3 + a_2 h^3}{12} + (a_1 - a_2)b\left(y_s - \frac{b}{2}\right)^2 + a_2 h\left(y_s - \frac{h}{2}\right)^2 \tag{6}$$

$$I_y = \frac{b(a_1 - a_2)^3 + h{a_2}^3}{12} + a_2 h\left(x_d - \frac{a_2}{2}\right)^2 + (a_1 - a_2)b\left(a_1 - x_d - \frac{a_1 - a_2}{2}\right)^2 \tag{7}$$

The resultant force and resultant moments are

$$R = P_1 + P_2 + P_3 \tag{8}$$

$$M_{xT} = M_{x1} + M_{x2} + M_{x3} + (P_1 + P_2)(y_s - y_1) - P_3(h - y_s - y_2) \tag{9}$$

$$M_{yT} = M_{y1} + M_{y2} + M_{y3} + (P_1 + P_3)(x_d - x_1) - P_2(a_1 - x_d - x_2) \tag{10}$$

2.1 The maximum pressure is located at the corner of the footing

Fig. 2 shows the eleven possible cases, when the maximum pressure is found at the corner of the corner combined footing subjected to biaxial bending.

Case I considers that the area footing in contact with the soil works totally under compression. The pressure generated by the soil at any point of the footing "σ_z" is obtained by the biaxial bending general equation

$$\sigma_z = \frac{R}{A} + \frac{M_{xT} y}{I_x} + \frac{M_{yT} x}{I_y} \tag{11}$$

where: R is the resultant force, M_{xT} and M_{yT} are the resultant moments in the X and Y axes, A is the area or surface of contact of the footing with the soil, I_x and I_y are the moments of inertia on the X and Y axes, x and y are the coordinates at any point of the footing.

Cases II to XI consider that the area footing in contact with the soil works partially under compression. The pressure generated by the soil on the footing is obtained by the general equation of the pressure plane, from three known points.

Now for this case the three known points of the pressure plane are

$$\begin{aligned} &P_1(x_d, y_s, \sigma_{max}); \\ &P_2(x_d - a_3, y_s, 0); \\ &P_3(x_d, y_s - h_1, 0) \end{aligned} \tag{12}$$

where: σ_{max} is the available bearing capacity of the soil.

The general equation of the pressure plane can be obtained as follows

$$\begin{vmatrix} x - x_d & y - y_s & \sigma_z - \sigma_{max} \\ x_d - a_3 - x_d & y_s - y_s & 0 - \sigma_{max} \\ x_d - x_d & y_s - h_1 - y_s & 0 - \sigma_{max} \end{vmatrix} \tag{13}$$

Solving the determinant and the value of σ_z is obtained

$$\sigma_z = \frac{\sigma_{max}[(a_3 + x - x_d)h_1 + (y - y_s)a_3]}{a_3 h_1} \tag{14}$$

Case I

By Eq. (11) six general equations of soil pressure are obtained at each corner of the footing subject to biaxial bending

$$\sigma_1 = \frac{R}{A} + \frac{M_{xT} y_s}{I_x} + \frac{M_{yT} x_d}{I_y} \tag{15}$$

$$\sigma_2 = \frac{R}{A} + \frac{M_{xT} y_s}{I_x} + \frac{M_{yT}(x_d - a_1)}{I_y} \tag{16}$$

$$\sigma_3 = \frac{R}{A} + \frac{M_{xT}(y_s - b)}{I_x} + \frac{M_{yT}(x_d - a_2)}{I_y} \tag{17}$$

$$\sigma_4 = \frac{R}{A} + \frac{M_{xT}(y_s - b)}{I_x} + \frac{M_{yT}(x_d - a_1)}{I_y} \tag{18}$$

$$\sigma_5 = \frac{R}{A} + \frac{M_{xT}(y_s - h)}{I_x} + \frac{M_{yT} x_d}{I_y} \tag{19}$$

$$\sigma_6 = \frac{R}{A} + \frac{M_{xT}(y_s - h)}{I_x} + \frac{M_{yT}(x_d - a_2)}{I_y} \tag{20}$$

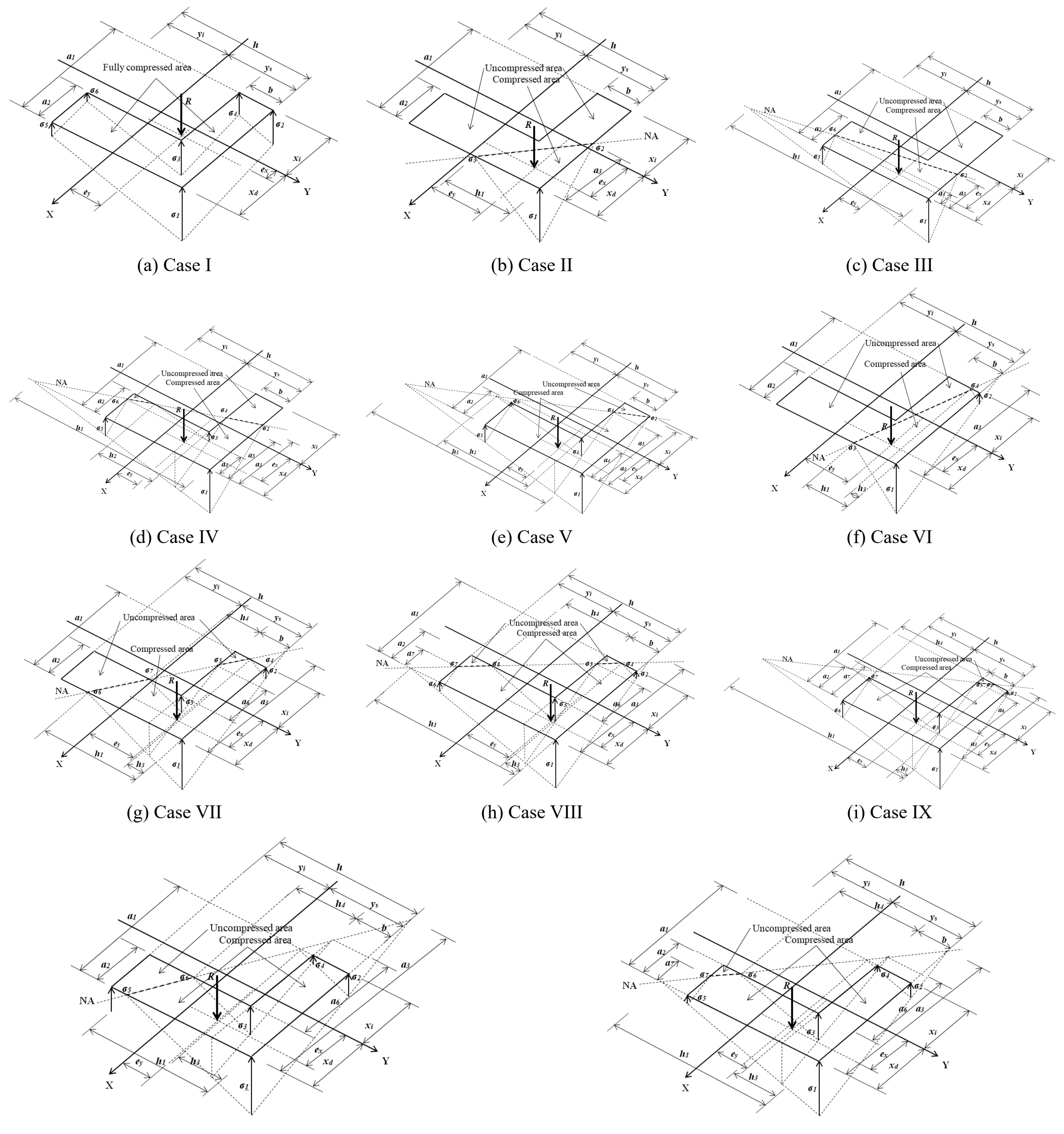

(a) Case I (b) Case II (c) Case III

(d) Case IV (e) Case V (f) Case VI

(g) Case VII (h) Case VIII (i) Case IX

(j) Case X (k) Case XI

Fig. 2 Corner combined footing subjected to biaxial bending (Maximum pressure is found at the corner)

Case II

The general equations of the resultant force "R", the resultant moment on the X axis "M_{xT}" and the resultant moment on the Y axis "M_{yT}" are obtained as follows

$$R = \int_{y_s-h_1}^{y_s} \int_{x_d+\frac{a_3(y_s-y)}{h_1}-a_3}^{x_d} \sigma_z dxdy \tag{21}$$

$$R = \frac{\sigma_{max} a_3 h_1}{6} \tag{22}$$

$$M_{xT} = \int_{y_s-h_1}^{y_s} \int_{x_d+\frac{a_3(y_s-y)}{h_1}-a_3}^{x_d} \sigma_z ydxdy \tag{23}$$

$$M_{xT} = \frac{\sigma_{max} a_3 h_1 (4y_s - h_1)}{24} \tag{24}$$

$$M_{yT} = \int_{y_s-h_1}^{y_s} \int_{x_d+\frac{a_3(y_s-y)}{h_1}-a_3}^{x_d} \sigma_z xdxdy \tag{25}$$

$$M_{yT} = \frac{\sigma_{max} a_3 h_1 (4x_d - a_3)}{24} \tag{26}$$

Case III

The general equations of the resultant force "R", the resultant moment on the X axis "M_{xT}" and the resultant moment on the Y axis "M_{yT}" are obtained as follows

$$R = \int_{y_s-h}^{y_s} \int_{x_d+\frac{a_3(y_s-y)}{h_1}-a_3}^{x_d} \sigma_z dxdy \tag{27}$$

$$R = \frac{\sigma_{max} a_3 \left[{h_1}^3 - (h_1 - h)^3\right]}{6{h_1}^2} \tag{28}$$

$$M_{xT} = \int_{y_s-h}^{y_s} \int_{x_d+\frac{a_3(y_s-y)}{h_1}-a_3}^{x_d} \sigma_z ydxdy \tag{29}$$

$$M_{xT} = \frac{\sigma_{max} a_3}{24{h_1}^2}\left[{h_1}^3(4y_s - h_1) - (h_1 - h)^3(4y_s - 3h - h_1)\right] \tag{30}$$

$$M_{yT} = \int_{y_s-h}^{y_s} \int_{x_d+\frac{a_3(y_s-y)}{h_1}-a_3}^{x_d} \sigma_z xdxdy \tag{31}$$

$$M_{yT} = \frac{\sigma_{max} a_3}{24{h_1}^3}\left\{{h_1}^4(4x_d - a_3) - (h_1 - h)^3[4x_d h_1 - (h_1 - h)a_3]\right\} \tag{32}$$

Case IV

The general equations of the resultant force "R", the resultant moment on the X axis "M_{xT}" and the resultant moment on the Y axis "M_{yT}" are obtained as follows

$$R = -\int_{y_s-b-\frac{a_3(h_1-b)-a_2h_1}{a_3}}^{y_s-b} \int_{x_d+\frac{a_3(y_s-y)}{h_1}-a_3}^{x_d-a_2} \sigma_z dxdy + \int_{y_s-h}^{y_s} \int_{x_d+\frac{a_3(y_s-y)}{h_1}-a_3}^{x_d} \sigma_z dxdy \tag{33}$$

$$R = \frac{\sigma_{max}}{6{a_3}^2{h_1}^2}\left\{{a_3}^3\left[{h_1}^3 - (h_1 - h)^3\right] - [(a_3 - a_2)h_1 - a_3 b]^3\right\} \tag{34}$$

$$M_{xT} = -\int_{y_s-b-\frac{a_3(h_1-b)-a_2h_1}{a_3}}^{y_s-b} \int_{x_d+\frac{a_3(y_s-y)}{h_1}-a_3}^{x_d-a_2} \sigma_z ydxdy + \int_{y_s-h}^{y_s} \int_{x_d+\frac{a_3(y_s-y)}{h_1}-a_3}^{x_d} \sigma_z ydxdy \tag{35}$$

$$\begin{aligned} M_{xT} = \frac{\sigma_{max}}{24{a_3}^3{h_1}^2}\{&{a_3}^4{h_1}^3(4y_s - h_1) - {a_3}^4(h_1 - h)^3(4y_s - 3h - h_1) \\ &- [(a_3 - a_2)h_1 - a_3 b]^3[(4y_s - 3b - h_1)a_3 + a_2 h_1]\} \end{aligned} \tag{36}$$

$$M_{yT} = -\int_{y_s-b-\frac{a_3(h_1-b)-a_2h_1}{a_3}}^{y_s-b} \int_{x_d+\frac{a_3(y_s-y)}{h_1}-a_3}^{x_d-a_2} \sigma_z xdxdy + \int_{y_s-h}^{y_s} \int_{x_d+\frac{a_3(y_s-y)}{h_1}-a_3}^{x_d} \sigma_z xdxdy \tag{37}$$

$$\begin{aligned} M_{yT} = \frac{\sigma_{max}}{24{a_3}^2{h_1}^3}\{&[a_3 b - (a_3 - a_2)h_1]^3[(4x_d - 3a_2 - a_3)h_1 + a_3 b] + {a_3}^3{h_1}^4(4x_d - a_3) \\ &- {a_3}^3(h_1 - h)^3[4x_d h_1 - a_3(h_1 - h)]\} \end{aligned} \tag{38}$$

Case V

The general equations of the resultant force "R", the resultant moment on the X axis "M_{xT}" and the resultant moment on the Y axis "M_{yT}" are obtained as follows

$$R=\int_{y_s-h}^{y_s}\int_{x_d+\frac{a_3(y_s-y)}{h_1}-a_3}^{x_d}\sigma_z dxdy-\int_{y_s-h}^{y_s-b}\int_{x_d+\frac{a_3(y_s-y)}{h_1}-a_3}^{x_d-a_2}\sigma_z dxdy \tag{39}$$

$$R=\frac{\sigma_{max}}{6a_3{}^2h_1{}^2}\left\{a_3{}^3\left[h_1{}^3-(h_1-h)^3\right]-[(a_3-a_2)h_1-a_3b]^3+[(a_3-a_2)h_1-a_3h]^3\right\} \tag{40}$$

$$M_{xT}=\int_{y_s-h}^{y_s}\int_{x_d+\frac{a_3(y_s-y)}{h_1}-a_3}^{x_d}\sigma_z ydxdy-\int_{y_s-h}^{y_s-b}\int_{x_d+\frac{a_3(y_s-y)}{h_1}-a_3}^{x_d-a_2}\sigma_z ydxdy \tag{41}$$

$$\begin{aligned}M_{xT}=\frac{\sigma_{max}}{24a_3{}^3h_1{}^2}&\left\{a_3{}^4h_1{}^3(4y_s-h_1)-a_3{}^4(h_1-h)^3(4y_s-3h-h_1)\right.\\&-[(a_3-a_2)h_1-a_3b]^3[(4y_s-3b-h_1)a_3+a_2h_1]\\&\left.+[(a_3-a_2)h_1-a_3h]^3[(4y_s-3h-h_1)a_3+a_2h_1]\right\}\end{aligned} \tag{42}$$

$$M_{yT}=\int_{y_s-h}^{y_s}\int_{x_d+\frac{a_3(y_s-y)}{h_1}-a_3}^{x_d}\sigma_z xdxdy-\int_{y_s-h}^{y_s-b}\int_{x_d+\frac{a_3(y_s-y)}{h_1}-a_3}^{x_d-a_2}\sigma_z xdxdy \tag{43}$$

$$\begin{aligned}M_{yT}=\frac{\sigma_{max}}{24a_3{}^2h_1{}^3}&\left\{a_3{}^3h_1{}^4(4x_d-a_3)-a_3{}^3(h_1-h)^3[4x_dh_1-a_3(h_1-h)]\right.\\&-[(a_3-a_2)h_1-a_3b]^3[(4x_d-3a_2-a_3)h_1+a_3b]\\&\left.+[(a_3-a_2)h_1-a_3h]^3[(4x_d-3a_2-a_3)h_1+a_3h]\right\}\end{aligned} \tag{44}$$

Case VI

The general equations of the resultant force “R”, the resultant moment on the X axis “M_{xT}” and the resultant moment on the Y axis “M_{yT}” are obtained as follows

$$R=\int_{x_d-a_1}^{x_d}\int_{y_s+\frac{h_1(x_d-x)}{a_3}-h_1}^{y_s}\sigma_z dydx \tag{45}$$

$$R=\frac{\sigma_{max}h_1[a_3{}^3-(a_3-a_1)^3]}{6a_3{}^2} \tag{46}$$

$$M_{xT}=\int_{x_d-a_1}^{x_d}\int_{y_s+\frac{h_1(x_d-x)}{a_3}-h_1}^{y_s}\sigma_z ydydx \tag{47}$$

$$M_{xT}=\frac{\sigma_{max}h_1}{24a_3{}^3}\{a_3{}^4(4y_s-h_1)-(a_3-a_1)^3[4a_3y_s-(a_3-a_1)h_1]\} \tag{48}$$

$$M_{yT}=\int_{x_d-a_1}^{x_d}\int_{y_s+\frac{h_1(x_d-x)}{a_3}-h_1}^{y_s}\sigma_z xdydx \tag{49}$$

$$M_{yT}=\frac{\sigma_{max}h_1}{24a_3{}^2}[a_3{}^3(4x_d-a_3)-(a_3-a_1)^3(4x_d-a_3-3a_1)] \tag{50}$$

Case VII

The general equations of the resultant force “R”, the resultant moment on the X axis “M_{xT}” and the resultant moment on the Y axis “M_{yT}” are obtained as follows

$$R=-\int_{x_d-a_2-\frac{h_1(a_3-a_2)-a_3b}{h_1}}^{x_d-a_2}\int_{y_s+\frac{h_1(x_d-x)}{a_3}-h_1}^{y_s-b}\sigma_z dydx+\int_{x_d-a_1}^{x_d}\int_{y_s+\frac{h_1(x_d-x)}{a_3}-h_1}^{y_s}\sigma_z dydx \tag{51}$$

$$R=\frac{\sigma_{max}}{6a_3{}^2h_1{}^2}\left[a_3{}^3h_1{}^3-h_1{}^3(a_3-a_1)^3-[h_1(a_3-a_2)-a_3b]^3\right] \tag{52}$$

$$M_{xT} = -\int_{x_d - a_2 - \frac{h_1(a_3-a_2)-a_3 b}{h_1}}^{x_d - a_2} \int_{y_s + \frac{h_1(x_d - x)}{a_3} - h_1}^{y_s - b} \sigma_z y dy dx + \int_{x_d - a_1}^{x_d} \int_{y_s + \frac{h_1(x_d - x)}{a_3} - h_1}^{y_s} \sigma_z y dy dx \tag{53}$$

$$M_{xT} = \frac{\sigma_{max}}{24 a_3{}^3 h_1{}^2} \{ a_3{}^4 h_1{}^3 (4y_s - h_1) - h_1{}^3 (a_3 - a_1)^3 [4a_3 y_s - (a_3 - a_1)h_1] - [h_1(a_3 - a_2) - a_3 b]^3 [(4y_s - 3b - h_1)a_3 + a_2 h_1] \} \tag{54}$$

$$M_{yT} = -\int_{x_d - a_2 - \frac{h_1(a_3-a_2)-a_3 b}{h_1}}^{x_d - a_2} \int_{y_s + \frac{h_1(x_d - x)}{a_3} - h_1}^{y_s - b} \sigma_z x dy dx + \int_{x_d - a_1}^{x_d} \int_{y_s + \frac{h_1(x_d - x)}{a_3} - h_1}^{y_s} \sigma_z x dy dx \tag{55}$$

$$M_{yT} = \frac{\sigma_{max}}{24 a_3{}^2 h_1{}^3} \{ a_3{}^3 h_1{}^4 (4x_d - a_3) - h_1{}^4 (a_3 - a_1)^3 (4x_d - a_3 - 3a_1) - [h_1(a_3 - a_2) - a_3 b]^3 [(4x_d - 3a_2 - a_3)h_1 + a_3 b] \} \tag{56}$$

Case VIII

The general equations of the resultant force "R", the resultant moment on the X axis "M_{xT}" and the resultant moment on the Y axis "M_{yT}" are obtained as follows

$$R = -\int_{x_d - a_2 - \frac{h_1(a_3-a_2)-a_3 b}{h_1}}^{x_d - a_2} \int_{y_s + \frac{h_1(x_d - x)}{a_3} - h_1}^{y_s - b} \sigma_z dy dx - \int_{x_d - \frac{a_3(h_1 - h)}{h_1}}^{x_d} \int_{y_s + \frac{h_1(x_d - x)}{a_3} - h_1}^{y_s - h} \sigma_z dy dx + \int_{x_d - a_1}^{x_d} \int_{y_s + \frac{h_1(x_d - x)}{a_3} - h_1}^{y_s} \sigma_z dy dx \tag{57}$$

$$R = \frac{\sigma_{max}}{6 a_3{}^2 h_1{}^2} \{ a_3{}^3 h_1{}^3 - h_1{}^3 (a_3 - a_1)^3 - [h_1(a_3 - a_2) - a_3 b]^3 - a_3{}^3 (h_1 - h)^3 \} \tag{58}$$

$$M_{xT} = -\int_{x_d - a_2 - \frac{h_1(a_3-a_2)-a_3 b}{h_1}}^{x_d - a_2} \int_{y_s + \frac{h_1(x_d - x)}{a_3} - h_1}^{y_s - b} \sigma_z y dy dx - \int_{x_d - \frac{a_3(h_1 - h)}{h_1}}^{x_d} \int_{y_s + \frac{h_1(x_d - x)}{a_3} - h_1}^{y_s - h} \sigma_z y dy dx + \int_{x_d - a_1}^{x_d} \int_{y_s + \frac{h_1(x_d - x)}{a_3} - h_1}^{y_s} \sigma_z y dy dx \tag{59}$$

$$M_{xT} = \frac{\sigma_{max}}{24 a_3{}^3 h_1{}^2} \{ a_3{}^4 h_1{}^3 (4y_s - h_1) - h_1{}^3 (a_3 - a_1)^3 [4a_3 y_s - (a_3 - a_1)h_1] - a_3{}^4 (h_1 - h)^3 (4y_s - 3h - h_1) - [h_1(a_3 - a_2) - a_3 b]^3 [(4y_s - 3b - h_1)a_3 + a_2 h_1] \} \tag{60}$$

$$M_{yT} = -\int_{x_d - a_2 - \frac{h_1(a_3-a_2)-a_3 b}{h_1}}^{x_d - a_2} \int_{y_s + \frac{h_1(x_d - x)}{a_3} - h_1}^{y_s - b} \sigma_z x dy dx - \int_{x_d - \frac{a_3(h_1 - h)}{h_1}}^{x_d} \int_{y_s + \frac{h_1(x_d - x)}{a_3} - h_1}^{y_s - h} \sigma_z x dy dx + \int_{x_d - a_1}^{x_d} \int_{y_s + \frac{h_1(x_d - x)}{a_3} - h_1}^{y_s} \sigma_z x dy dx \tag{61}$$

$$M_{yT} = \frac{\sigma_{max}}{24 a_3{}^2 h_1{}^3} \{ a_3{}^3 h_1{}^4 (4x_d - a_3) - h_1{}^4 (a_3 - a_1)^3 (4x_d - a_3 - 3a_1) - a_3{}^3 (h_1 - h)^3 [4x_d h_1 - (h_1 - h)a_3] - [h_1(a_3 - a_2) - a_3 b]^3 [(4x_d - 3a_2 - a_3)h_1 + a_3 b] \} \tag{62}$$

Case IX

The general equations of the resultant force "R", the resultant moment on the X axis "M_{xT}" and the resultant moment on the Y axis "M_{yT}" are obtained as follows

$$R = -\int_{x_d - a_2 - \frac{h_1(a_3-a_2)-a_3 b}{h_1}}^{x_d - a_2} \int_{y_s + \frac{h_1(x_d - x)}{a_3} - h_1}^{y_s - b} \sigma_z dy dx - \int_{x_d - \frac{a_3(h_1 - h)}{h_1}}^{x_d} \int_{y_s + \frac{h_1(x_d - x)}{a_3} - h_1}^{y_s - h} \sigma_z dy dx + \int_{x_d - \frac{a_3(h_1 - h)}{h_1}}^{x_d - a_2} \int_{y_s + \frac{h_1(x_d - x)}{a_3} - h_1}^{y_s - h} \sigma_z dy dx + \int_{x_d - a_1}^{x_d} \int_{y_s + \frac{h_1(x_d - x)}{a_3} - h_1}^{y_s} \sigma_z dy dx \tag{63}$$

$$R = \frac{\sigma_{max}}{6{a_3}^2{h_1}^2}\{{a_3}^3{h_1}^3 - {h_1}^3(a_3 - a_1)^3 - [h_1(a_3 - a_2) - a_3 b]^3 - {a_3}^3(h_1 - h)^3 + [h_1(a_3 - a_2) - a_3 h]^3\} \quad (64)$$

$$\begin{aligned} M_{xT} = &- \int_{x_d - a_2 - \frac{h_1(a_3 - a_2) - a_3 b}{h_1}}^{x_d - a_2} \int_{y_s + \frac{h_1(x_d - x)}{a_3} - h_1}^{y_s - b} \sigma_z y dy dx - \int_{x_d - \frac{a_3(h_1 - h)}{h_1}}^{x_d} \int_{y_s + \frac{h_1(x_d - x)}{a_3} - h_1}^{y_s - h} \sigma_z y dy dx \\ &+ \int_{x_d - \frac{a_3(h_1 - h)}{h_1}}^{x_d - a_2} \int_{y_s + \frac{h_1(x_d - x)}{a_3} - h_1}^{y_s - h} \sigma_z y dy dx + \int_{x_d - a_1}^{x_d} \int_{y_s + \frac{h_1(x_d - x)}{a_3} - h_1}^{y_s} \sigma_z y dy dx \end{aligned} \quad (65)$$

$$\begin{aligned} M_{xT} = \frac{\sigma_{max}}{24{a_3}^3{h_1}^2}\{&{a_3}^4{h_1}^3(4y_s - h_1) - {h_1}^3(a_3 - a_1)^3[4a_3 y_s - (a_3 - a_1)h_1] - {a_3}^4(h_1 - h)^3(4y_s - 3h - h_1) \\ &- [h_1(a_3 - a_2) - a_3 b]^3[(4y_s - 3b - h_1)a_3 + a_2 h_1] \\ &+ [h_1(a_3 - a_2) - a_3 h]^3[(4y_s - 3h - h_1)a_3 + a_2 h_1]\} \end{aligned} \quad (66)$$

$$\begin{aligned} M_{yT} = &- \int_{x_d - a_2 - \frac{h_1(a_3 - a_2) - a_3 b}{h_1}}^{x_d - a_2} \int_{y_s + \frac{h_1(x_d - x)}{a_3} - h_1}^{y_s - b} \sigma_z x dy dx - \int_{x_d - \frac{a_3(h_1 - h)}{h_1}}^{x_d} \int_{y_s + \frac{h_1(x_d - x)}{a_3} - h_1}^{y_s - h} \sigma_z x dy dx \\ &+ \int_{x_d - \frac{a_3(h_1 - h)}{h_1}}^{x_d - a_2} \int_{y_s + \frac{h_1(x_d - x)}{a_3} - h_1}^{y_s - h} \sigma_z x dy dx + \int_{x_d - a_1}^{x_d} \int_{y_s + \frac{h_1(x_d - x)}{a_3} - h_1}^{y_s} \sigma_z x dy dx \end{aligned} \quad (67)$$

$$\begin{aligned} M_{yT} = \frac{\sigma_{max}}{24{a_3}^2{h_1}^3}\{&{a_3}^3{h_1}^4(4x_d - a_3) - {h_1}^4(a_3 - a_1)^3(4x_d - a_3 - 3a_1) - {a_3}^3(h_1 - h)^3[4x_d h_1 - (h_1 - h)a_3] \\ &- [h_1(a_3 - a_2) - a_3 b]^3[(4x_d - 3a_2 - a_3)h_1 + a_3 b] \\ &+ [h_1(a_3 - a_2) - a_3 h]^3[(4x_d - 3a_2 - a_3)h_1 + a_3 h]\} \end{aligned} \quad (68)$$

Case X

The general equations of the resultant force "R", the resultant moment on the X axis "M_{xT}" and the resultant moment on the Y axis "M_{yT}" are obtained as follows

$$R = \int_{x_d - a_1}^{x_d} \int_{y_s + \frac{h_1(x_d - x)}{a_3} - h_1}^{y_s} \sigma_z dy dx - \int_{x_d - a_1}^{x_d - a_2} \int_{y_s + \frac{h_1(x_d - x)}{a_3} - h_1}^{y_s - b} \sigma_z dy dx \quad (69)$$

$$R = \frac{\sigma_{max}}{6{a_3}^2{h_1}^2}\{{a_3}^3{h_1}^3 - {h_1}^3(a_3 - a_1)^3 - [h_1(a_3 - a_2) - a_3 b]^3 + [h_1(a_3 - a_1) - a_3 b]^3\} \quad (70)$$

$$M_{xT} = \int_{x_d - a_1}^{x_d} \int_{y_s + \frac{h_1(x_d - x)}{a_3} - h_1}^{y_s} \sigma_z y dy dx - \int_{x_d - a_1}^{x_d - a_2} \int_{y_s + \frac{h_1(x_d - x)}{a_3} - h_1}^{y_s - b} \sigma_z y dy dx \quad (71)$$

$$\begin{aligned} M_{xT} = \frac{\sigma_{max}}{24{a_3}^3{h_1}^2}\{&{a_3}^4{h_1}^3(4y_s - h_1) - {h_1}^3(a_3 - a_1)^3[4a_3 y_s - (a_3 - a_1)h_1] \\ &- [h_1(a_3 - a_2) - a_3 b]^3[(4y_s - 3b - h_1)a_3 + a_2 h_1] \\ &+ [h_1(a_3 - a_1) - a_3 b]^3[(4y_s - 3b - h_1)a_3 + a_1 h_1]\} \end{aligned} \quad (72)$$

$$M_{yT} = \int_{x_d - a_1}^{x_d} \int_{y_s + \frac{h_1(x_d - x)}{a_3} - h_1}^{y_s} \sigma_z x dy dx - \int_{x_d - a_1}^{x_d - a_2} \int_{y_s + \frac{h_1(x_d - x)}{a_3} - h_1}^{y_s - b} \sigma_z x dy dx \quad (73)$$

$$\begin{aligned} M_{yT} = \frac{\sigma_{max}}{24{a_3}^2{h_1}^3}\{&{a_3}^3{h_1}^4(4x_d - a_3) - {h_1}^4(a_3 - a_1)^3(4x_d - a_3 - 3a_1) \\ &- [h_1(a_3 - a_2) - a_3 b]^3[(4x_d - 3a_2 - a_3)h_1 + a_3 b] \\ &+ [h_1(a_3 - a_1) - a_3 b]^3[(4x_d - 3a_1 - a_3)h_1 + a_3 b]\} \end{aligned} \quad (74)$$

Case XI

The general equations of the resultant force "R", the resultant moment on the X axis "M_{xT}" and the resultant moment on the Y axis "M_{yT}" are obtained as follows

Table 1 Constraint functions when the maximum pressure is located at the corner of the footing

Case	Constraint functions and conditions
I	Eqs. (1), (2), (4), (6) to (10), (15) to (20), $0 \leq \sigma_1, \sigma_2, \sigma_3, \sigma_4, \sigma_5, \sigma_6 \leq \sigma_{max}$
II	Eqs. (2), (4), (8) to (10), (22), (24), (26), $a_1 \geq a_3$, $a_2 \geq a_3(h_1 - b)/h_1$, $h \geq h_1$
III	Eqs. (2), (4), (8) to (10), (28), (30), (32), $a_1 \geq a_3$, $a_2 \geq a_3(h_1 - b)/h_1$, $a_2 \leq a_3(h_1 - h)/h_1$, $h_1 \geq h$
IV	Eqs. (2), (4), (8) to (10), (34), (36), (38), $a_1 \geq a_3$, $a_2 \leq a_3(h_1 - b)/h_1$, $a_2 \geq a_3(h_1 - h)/h_1$, $h_1 \geq h$
V	Eqs. (2), (4), (8) to (10), (40), (42), (44), $a_1 \geq a_3$, $a_2 \leq a_3(h_1 - b)/h_1$, $a_2 \leq a_3(h_1 - h)/h_1$, $h_1 \geq h$
VI	Eqs. (2), (4), (8) to (10), (46), (48), (50), $a_1 \leq a_3$, $a_2 \geq a_3(h_1 - b)/h_1$, $h_1 \leq h$
VII	Eqs. (2), (4), (8) to (10), (52), (54), (56), $a_1 \leq a_3$, $a_2 \leq a_3(h_1 - b)/h_1$, $h_1 \leq h$
VIII	Eqs. (2), (4), (8) to (10), (58), (60), (62), $a_1 \leq a_3$, $a_2 \leq a_3(h_1 - b)/h_1$, $a_2 \geq a_3(h_1 - h)/h_1$, $h_1 \geq h$
IX	Eqs. (2), (4), (8) to (10), (64), (66), (68), $a_1 \leq a_3$, $a_2 \leq a_3(h_1 - b)/h_1$, $a_2 \leq a_3(h_1 - h)/h_1$, $h_1 \geq h$
X	Eqs. (2), (4), (8) to (10), (70), (72), (74), $a_1 \leq a_3$, $a_1 \leq a_3(h_1 - b)/h_1$, $h_1 \leq h$
XI	Eqs. (2), (4), (8) to (10), (76), (78), (80), $a_1 \leq a_3$, $a_1 \leq a_3(h_1 - b)/h_1$, $a_2 \geq a_3(h_1 - h)/h_1$, $h_1 \geq h$

*Note: In all cases, the following conditions must be added: $h = y_1 + L_y + y_2$, $a_1 = x_1 + L_x + x_2$, $a_1 \geq a_2$, and $h \geq b$

$$\begin{aligned} R = &-\int_{x_d-\frac{a_3(h_1-h)}{h_1}}^{x_d}\int_{y_s+\frac{h_1(x_d-x)}{a_3}-h_1}^{y_s-h}\sigma_z dydx-\int_{x_d-a_1}^{x_d-a_2}\int_{y_s+\frac{h_1(x_d-x)}{a_3}-h_1}^{y_s-b}\sigma_z dydx\\ &+\int_{x_d-a_1}^{x_d}\int_{y_s+\frac{h_1(x_d-x)}{a_3}-h_1}^{y_s}\sigma_z dydx \end{aligned} \tag{75}$$

$$R=\frac{\sigma_{max}}{6a_3^2h_1^2}\left\{a_3^3h_1^3-h_1^3(a_3-a_1)^3-a_3^3(h_1-h)^3-[h_1(a_3-a_2)-a_3b]^3+[h_1(a_3-a_1)-a_3b]^3\right\} \tag{76}$$

$$\begin{aligned} M_{xT} = &-\int_{x_d-\frac{a_3(h_1-h)}{h_1}}^{x_d}\int_{y_s+\frac{h_1(x_d-x)}{a_3}-h_1}^{y_s-h}\sigma_z ydydx-\int_{x_d-a_1}^{x_d-a_2}\int_{y_s+\frac{h_1(x_d-x)}{a_3}-h_1}^{y_s-b}\sigma_z ydydx\\ &+\int_{x_d-a_1}^{x_d}\int_{y_s+\frac{h_1(x_d-x)}{a_3}-h_1}^{y_s}\sigma_z ydydx \end{aligned} \tag{77}$$

$$\begin{aligned} M_{xT} = \frac{\sigma_{max}}{24a_3^3h_1^2}&\left\{a_3^4h_1^3(4y_s-h_1)-a_3^4(h_1-h)^3(4y_s-3h-h_1)-h_1^3(a_3-a_1)^3[4a_3y_s-(a_3-a_1)h_1]\right.\\ &-[h_1(a_3-a_2)-a_3b]^3[(4y_s-3b-h_1)a_3+a_2h_1]\\ &\left.+[h_1(a_3-a_1)-a_3b]^3[(4y_s-3b-h_1)a_3+a_1h_1]\right\} \end{aligned} \tag{78}$$

$$M_{yT} = -\int_{x_d-\frac{a_3(h_1-h)}{h_1}}^{x_d}\int_{y_s+\frac{h_1(x_d-x)}{a_3}-h_1}^{y_s-h}\sigma_z xdydx-\int_{x_d-a_1}^{x_d-a_2}\int_{y_s+\frac{h_1(x_d-x)}{a_3}-h_1}^{y_s-b}\sigma_z xdydx \tag{79}$$

$$+\int_{x_d-a_1}^{x_d}\int_{y_s+\frac{h_1(x_d-x)}{a_3}-h_1}^{y_s}\sigma_z xdydx \tag{79}$$

$$\begin{aligned} M_{yT} = \frac{\sigma_{max}}{24a_3^2h_1^3}&\Big[a_3^3h_1^4(4x_d-a_3)-a_3^3(h_1-h)^3[(4x_d-a_3)h_1+a_3h]-h_1^4(a_3-a_1)^3(4x_d-a_3-3a_1)\\ &-[h_1(a_3-a_2)-a_3b]^3[(4x_d-3a_2-a_3)h_1+a_3b]\\ &+[h_1(a_3-a_1)-a_3b]^3[(4x_d-3a_1-a_3)h_1+a_3b]\Big] \end{aligned} \tag{80}$$

2.2 Minimum area for corner combined footings

The minimum area "A_{min}" (objective function) for all cases is

$$A_{min} = (a_1 - a_2)b + a_2h \tag{81}$$

Table 1 shows the constraint functions and conditions when the maximum pressure is located at the corner of the footing.

The procedure to obtain the location of the maximum pressure is using case I. Once the location of the maximum pressure is known, the corresponding constraint functions can be used.

Fig. 3 shows the flowchart using the equations proposed for each case and how to use Maple software to obtain the minimum area of a reinforced concrete corner combined footing (Nonlinear optimization).

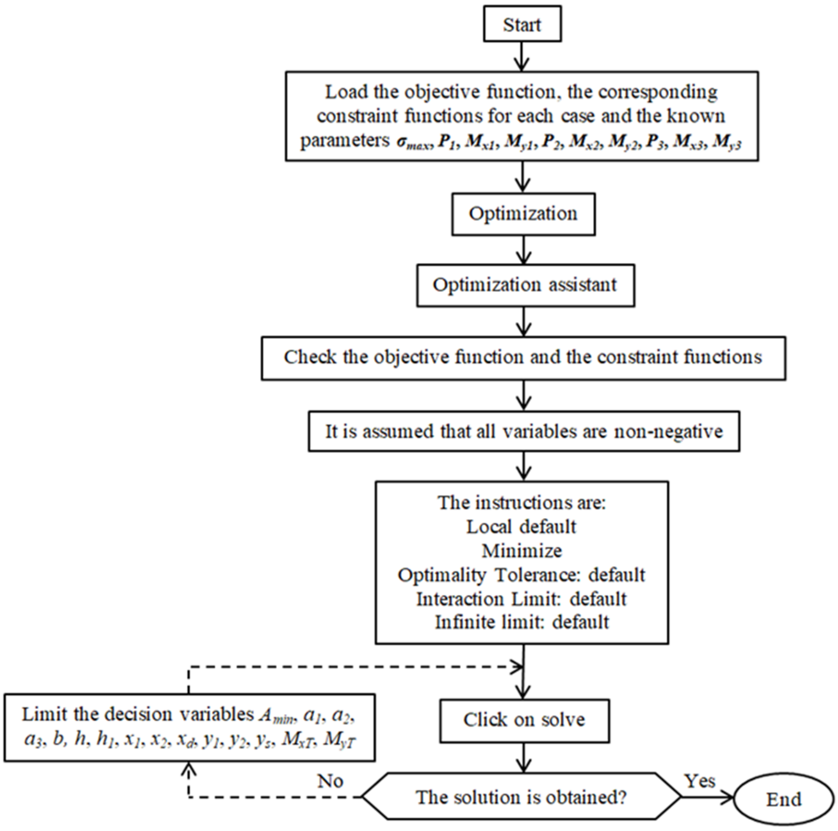

Fig. 3 Flowchart using the equations proposed for each case by Maple software for corner combined footing

Table 2 Minimum area with unlimited sides at the ends (x1 = 0.20, x2 ≥ 0.20, y1 = 0.20 and y2 ≥ 0.20)

P_1 (kN)	Case	σ_{max} (kN/m^2)	R (kN)	M_{xT} (kN-m)	M_{yT} (kN-m)	a_1 (m)	a_2 (m)	a_3 (m)	b (m)	h (m)	h_1 (m)	x_1 (m)	x_2 (m)	x_d (m)	y_1 (m)	y_2 (m)	y_s (m)	A_{min} (m^2)
600	I	250	1600	1040.00	540.00	5.40	1.00	-	1.00	6.40	-	0.20	0.20	1.60	0.20	0.20	2.10	10.80
	IX[a]		1600	869.81	860.04	5.59	1.00	10.96	1.21	6.40	7.76	0.20	0.39	1.80	0.20	0.20	1.99	11.96
	I	200	1600	1960.23	582.33	5.40	1.00	-	1.34	8.22	-	0.20	0.20	1.63	0.20	2.02	2.68	14.11
	IX[a]		1600	1083.53	1082.09	5.40	1.00	13.12	1.82	7.03	7.99	0.20	0.20	1.94	0.20	0.83	2.13	15.05
	I	150	1600	2474.91	3077.49	11.08	1.00	-	1.00	10.70	-	0.20	5.88	3.19	0.20	4.50	3.00	20.77
	IX[a]		1600	2478.16	820.34	5.40	1.16	11.19	1.99	9.18	17.00	0.20	0.20	1.78	0.20	2.98	3.00	19.10
	I	100	No solution available															
	IX[a]		1600	2926.51	1462.10	5.40	1.00	14.57	4.00	10.75	18.00	0.20	0.20	2.18	0.20	4.55	3.28	28.35
400	I	250	1400	660.00	260.00	5.40	1.00	-	1.00	6.40	-	0.20	0.20	1.60	0.20	0.20	2.10	10.80
	IX[a]		1400	547.93	546.09	5.97	1.00	7.11	1.00	6.40	7.97	0.20	0.77	1.80	0.20	0.20	2.02	11.37
	I	200	1400	660.00	260.00	5.40	1.00	-	1.00	6.40	-	0.20	0.20	1.60	0.20	0.20	2.10	10.80
	IX[a]		1400	1053.17	166.94	5.40	1.00	7.30	1.00	7.09	13.91	0.20	0.20	1.53	0.20	0.89	2.38	11.49
	I	150	1400	1685.67	336.12	5.40	1.00	-	1.49	8.78	-	0.20	0.20	1.65	0.20	2.58	2.83	15.34
	IX[a]		1400	1807.71	25.30	5.40	1.37	6.76	1.00	7.68	20.44	0.20	0.20	1.43	0.20	1.48	2.92	14.59
	I	100	1400	2743.12	3434.92	14.02	1.15	-	1.00	12.65	-	0.20	8.82	3.87	0.20	6.45	3.59	27.40
	IX[a]		1400	3244.09	0	5.58	1.83	6.93	1.00	9.39	33.09	0.20	0.38	1.41	0.20	3.19	3.95	20.94

[a] Maximum pressure located at the corner

Table 3 Minimum area with limited sides at the ends (x_1 = 0.20, x_2 = 0.20, y_1 = 0.20 and y_2 = 0.20)

P_1 (kN)	Case	σ_{max} (kN/m^2)	R (kN)	M_{xT} (kN-m)	M_{yT} (kN-m)	a_1 (m)	a_2 (m)	a_3 (m)	b (m)	h (m)	h_1 (m)	x_1 (m)	x_2 (m)	x_d (m)	y_1 (m)	y_2 (m)	y_s (m)	A_{min} (m^2)
600	I	250	1600	1040.00	540.00	5.40	1.00	-	1.00	6.40	-	0.20	0.20	1.60	0.20	0.20	2.10	10.80
	IX[a]		1600	856.62	856.59	5.40	1.00	8.96	1.35	6.40	7.31	0.20	0.20	1.80	0.20	0.20	1.99	12.32
	I	200	1600	1142.22	892.87	5.40	1.33	-	1.56	6.40	-	0.20	0.20	1.82	0.20	0.20	2.16	14.86
	IX[a]		1600	1033.76	1031.53	5.40	1.25	13.50	1.75	6.40	7.49	0.20	0.20	1.91	0.20	0.20	2.10	15.26
	I	150								No solution available								
	IX[a]		1600	1526.96	1290.49	5.40	1.95	18.52	2.46	6.40	9.59	0.20	0.20	2.07	0.20	0.20	2.40	21.00
	I	100								No solution available								
	IX[a]		1600	2397.75	2043.42	5.40	3.17	59.56	4.98	6.40	8.78	0.20	0.20	2.54	0.20	0.20	2.95	31.39
400	I	250	1400	660.00	260.00	5.40	1.00	-	1.00	6.40	-	0.20	0.20	1.60	0.20	0.20	2.10	10.80
	IX[a]		1400	511.54	511.41	5.40	1.00	6.23	1.31	6.40	7.85	0.20	0.20	1.78	0.20	0.20	1.99	12.17
	I	200	1400	660.00	260.00	5.40	1.00	-	1.00	6.40	-	0.20	0.20	1.60	0.20	0.20	2.10	10.80
	IX[a]		1400	814.04	209.34	5.40	1.15	7.77	1.00	6.40	12.29	0.20	0.20	1.56	0.20	0.20	2.21	11.60
	I	150	1400	827.86	630.18	5.40	1.47	-	1.72	6.40	-	0.20	0.20	1.86	0.20	0.20	2.22	16.15
	IX[a]		1400	1306.76	181.56	5.40	1.81	8.66	1.00	6.40	16.03	0.20	0.20	1.54	0.20	0.20	2.56	15.18
	I	100								No solution available								
	IX[a]		1400	1451.29	1267.50	5.40	2.57	25.72	3.61	6.40	9.42	0.20	0.20	2.32	0.20	0.20	2.67	26.66

[a] Maximum pressure located at the corner

The importance of this research is:

1) In many cases, the minimum area for corner combined footings is governed by the minimum pressure (zero pressure) and not the maximum pressure that the soil can withstand, since the soil cannot withstand tensions, this occurs when the area of contact with the ground works completely under compression.

2) When maximum pressure is reached, a smaller contact area with the ground is generated, which leads to a lower volume of earth extraction due to excavation to build the footing.

3. Numerical problems

Tables 2 and 3 present the minimum areas and the dimensions of the corner combined footings subjected to biaxial bending for case I (area works totally to compression) and the smaller of all other cases (area works partially to compression).

Table 2 shows the results (Example 1) for c_1, c_2, c_3, c_4 = 0.40 m, L_x = 5.00 m, L_y = 6.00 m, P_1 = 600, 400 kN, P_2 = 500 kN, P_3 = 500 kN, M_{x1} = 500 kN-m, M_{x2} = 250 kN-m, M_{x3} = 250 kN-m, M_{y1} = 400 kN-m, M_{y2} = 200 kN-m, M_{y3} = 200 kN-m and σ_{max} = 250, 200, 150, 100 kN/m^2. These examples are presented unlimited at the ends ($h = c_3/2 + L_y + y_2$, $a_1 = c_2/2 + L_x + x_2$).

Table 3 shows the results for the same loads and moments as in example 1, but limited at the ends ($h = c_3/2 + L_y + c_4/2$, $a_1 = c_1/2 + L_x + c_2/2$).

4. Results

Table 2 presents the following (unlimited sides at the ends). When P_1 = 600 kN and σ_{max} decreases (case I): M_{xT}, M_{yT}, h, A_{min} increase; a_1 is the same at σ_{max} = 250, 200 kN/m^2 and then increases; a_2 remains equal to all σ_{max}; b tends to increase and then decreases (there is no solution available for σ_{max} = 100 kN/m^2). When P_1 = 600 kN and σ_{max} decreases (case IX[a]): M_{xT}, h, A_{min} increase; M_{yT} tends to decrease up to σ_{max} = 200 kN/m^2 and then increases up to σ_{max} = 150 kN/m^2 and subsequently decreases; a_1 tends to decrease until σ_{max} = 200 kN/m^2 and then is constant; a_2 is the same at all σ_{max} except at σ_{max} = 150 kN/m^2; b tends to increase; the smaller minimum area appears at σ_{max} = 250 and 200 kN/m^2 for case I and for σ_{max} = 150 and 100 kN/m^2 in case IX[a] (Even in case I, there is no solution available for σ_{max} = 100 kN/m^2). When P_1 = 400 kN and σ_{max} decreases (case I): M_{xT}, M_{yT}, h, A_{min} are the same at σ_{max} = 250 and 200 kN/m^2 and then increases; a_1, a_2 are constant at σ_{max} = 250, 200 and 150 kN/m^2 and then increases; b is constant at all σ_{max} except at σ_{max} = 150 kN/m^2. When P_1 = 400 kN and σ_{max} decreases (case IX[a]): M_{xT}, h, A_{min} increase; M_{yT} tends to decrease; a_1 tends to decrease up to σ_{max} = 200 kN/m^2 and then is constant at σ_{max} = 200 and 150 kN/m^2 and then increases; a_2 is constant at σ_{max} = 250 and 200 kN/m^2 and then increases; b is constant at all σ_{max}; the smaller minimum area appears at σ_{max} = 250 and 200 kN/m^2 for case I and for σ_{max} = 150 and 100 kN/m^2 in case IX[a].

Table 3 shows the following (limited sides at the ends). When P_1 = 600 kN and σ_{max} decreases (case I): M_{xT}, M_{yT}, b, a_2, A_{min} increase; a_1 remains equal to all σ_{max}; h is equal to all σ_{max} (there is no solution available for σ_{max} = 150, 100 kN/m^2). When P_1 = 600 kN and σ_{max} decreases (case IX[a]):

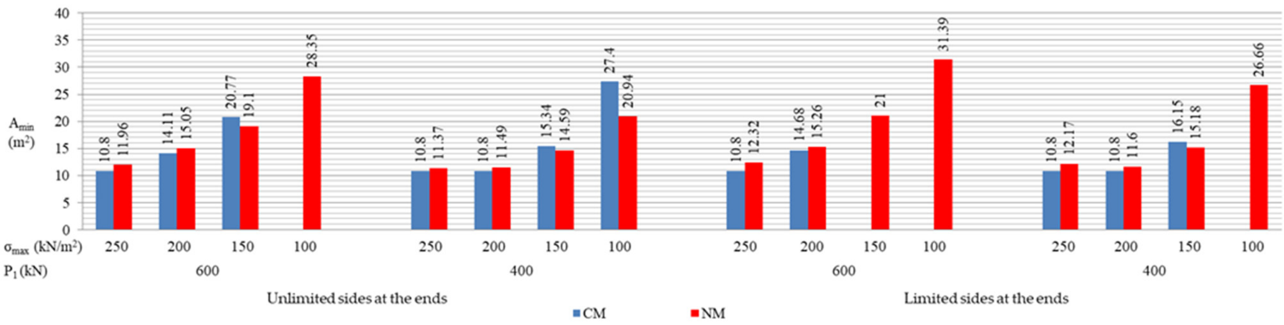

Fig. 4 Comparison of minimum areas of example 1

M_{xT}, M_{yT}, b, a_2, A_{min} increase; a_1, h remain equal to all σ_{max}; the smaller minimum area appears at σ_{max} = 250 and 200 kN/m^2 for case I and for σ_{max} = 150 and 100 kN/m^2 in case IX^a (Even in case I, there is no solution available for σ_{max} = 150, 100 kN/m^2). When P_1 = 400 kN and σ_{max} decreases (case I): M_{xT}, M_{yT}, b, a_2, A_{min} are the same at σ_{max} = 250 and 200 kN/m^2 and then increases; a_1, h remain equal to all σ_{max}. When P_1 = 400 kN and σ_{max} decreases (case IX^a): M_{xT}, a_2, A_{min} increase; M_{yT} tends to decrease up to σ_{max} = 150 kN/m^2 and subsequently increases; a_1 and h is constant at all σ_{max}; b tends to decrease up to σ_{max} = 200 kN/m^2 and is constant up to σ_{max} = 150 kN/m^2 and subsequently increases; the smaller minimum area appears at σ_{max} = 250 and 200 kN/m^2 for case I and for σ_{max} = 150 and 100 kN/m^2 in case IX^a (Even in case I, there is no solution available for σ_{max} = 100 kN/m^2).

Fig. 4 shows the comparison between the CM (Current Model) which is Case I (area works totally to compression) and the NM (New Model) which are all other cases (area works partially to compression) of example 1.

Fig. 4 shows the following: When σ_{max} decreases, the soil contact areas increase for both models. For σ_{max} = 250 and 200 kN/m^2 the Current Model is smaller and for σ_{max} = 150 and 100 kN/m^2 the New Model is smaller for both models. For σ_{max} = 250 kN/m^2 at P_1 = 600 kN of the Current Model presents the same area for unlimited and limited sides. For σ_{max} = 250 and 200 kN/m^2 at P_1 = 400 kN of the Current Model presents the same area for unlimited and limited sides. In some cases the current model does not appear. It is observed that to greater bearing capacity of the soil governs the current model, and to lower bearing capacity of the soil governs the new model.

5. Conclusions

This paper presents a mathematical model to obtain the optimal surface for corner combined footings subjected to biaxial bending in each column considering that the contact area with the ground works partially in compression, assuming that the soil pressure distribution is linear.

The optimal model is formulated from a mathematical approach based on a minimum area, and it is developed by integration to obtain the resultant force "R", resultant moment around the X axis "M_{xT}" and resultant moment around the Y axis "M_{yT}". The known or constant parameters (independent variables) are: σ_{max}, P_1, P_2, P_3, M_{x1}, M_{x2}, M_{x3}, M_{y1}, M_{y2} and M_{y3}. The unknown or decision variables (dependent variables) are: A_{min}, a_1, a_2, a_3, b, h, h_1, x_1, x_2, x_d, y_1, y_2, y_s, M_{xT} and M_{yT}.

This work will be of great help to structural engineers or foundation specialists, as it will enable them to fully design corner combined footings, i.e., to obtain the thickness and areas of reinforcing steel for the footings.

The main contributions shown in this paper are:

1.- This document shows the precise and simplified equations to obtain the minimum area, when the maximum pressure is located at the corner of the footing.

2.- The new model is always present and the current model does not appear in some cases for these examples (see Tables 2 and 3).

3.- The current model shows in some cases the same minimum area for case I, because it does not reach the maximum pressure nor the zero pressure (see Tables 2 and 3).

4.- When any of the resulting moments M_{xT} or M_{yT} are zero, it means that the resultant force is located on the X or Y axis as appropriate (see Table 2).

5.- In the new model, for example 1, case IX^a appears for unconstrained and constrained sides (see Tables 2 and 3).

The main advantage of this study is that it directly impacts the construction cost of footing, because by presenting less contact area with the soil, it generates less volume of footing filling.

Suggestions for future research include a new model for the optimal design of corner combined footings based on the footing dimensions shown in this paper assuming the contact surface works partially in compression.

References

Aguilera-Mancilla, G., Luévanos-Rojas, A., López-Chavarría, S. and Medina-Elizondo, M. (2019), "Modeling for the strap combined footings Part I: Optimal dimensioning", *Steel Compos. Struct., Int. J.*, **30**(2), 97-108. https://doi.org/10.12989/scs.2019.30.2.097

Al-Gahtani, H.J. and Adekunle, S.K. (2019), "A boundary-type approach for the computation of vertical stresses in soil due to arbitrarily shaped foundations", *World J. Eng.*, **16**(3), 419-426. https://doi.org/10.1108/WJE-02-2018-0051

Aydogdu, I. (2016), "New Iterative method to Calculate Base Stress of Footings under Biaxial Bending", *Int. J. Eng. Appl. Sci.* (*IJEAS*), **8**(4), 40-48. https://doi.org/10.24107/ijeas.281460

Bashir, M.A., Furuuchi, H., Ueda, T. and Bashir, N. (2013), "Prediction of ultimate moment anchorage capacity of concrete filled steel box footing", *Steel Compos*. *Struct*., *Int*. *J*., **15**(6), 645-658. https://doi.org/10.12989/scs.2013.15.6.645

Belabed, Z., Tounsi, A., Bousahla, A.A., Tounsi, A., Khedher, K.M. and Salem, M.A. (2024), "Mechanical behavior analysis of FG-CNTRC porous beams resting on Winkler and Pasternak elastic foundations: A finite element approach", *Comput*. *Concrete*, *Int*. *J*., **26**(3), 285-292. https://doi.org/10.12989/cac.2024.34.4.447

Bezmalinovic Colleoni, A.S. (2016), "Fórmulas Analíticas para la Presión de Contacto Lineal en Fundaciones Rectangulares Altamente Excéntricas", In: *IX Chilean Congress on Geotechnical Engineering*, Chilean Geotechnical Society, Universidad Austral de Chile, Chile.

Dai, W., Fatahizadeh, M., Touchaei, H.G., Moayedi, H. and Foong, L.K. (2023), "Application of six neural network-based solutions on bearing capacity of shallow footing on double-layer soils", *Steel Compos*. *Struct*., *Int*. *J*., **49**(2), 231-244. https://doi.org/10.12989/scs.2023.49.2.231

Galvis, F.A. and Smith-Pardo, P.J. (2020), "Axial load biaxial moment interaction (PMM) diagrams for shallow foundations: Design aids, experimental verification, and examples", *Eng*. *Struct*., **213**, p. 110582. https://doi.org/10.1016/j.engstruct.2020.110582

Girgin, K. (2017), "Simplified formulations for the determination of rotational spring constants in rigid spread footings resting on tensionless soil", *J*. *Civil Eng*. *Manag*., **23**(4), 464-474. https://doi.org/10.3846/13923730.2016.1210218

Gör, M. (2022), "Analyzing the bearing capacity of shallow foundations on two-layered soil using two novel cosmology-based optimization techniques", *Smart Struct*. *Syst*., *Int*. *J*., **29**(3), 513-522. https://doi.org/10.12989/sss.2022.29.3.513

Highter, W.H. and Anders, J.C. (1985), "Dimensioning footings subjected to eccentric loads", *J*. *Geotech*. *Eng*., **111**(5), 659-665. https://doi.org/10.1061/(ASCE)0733-9410(1985)111:5(659)

Himeur, N., Mamen, B., Benguediab, S., Bouhadra, A., Menasria, A., Bouchouicha, B., Bourada, F., Benguediab, M. and Tounsi, A. (2022), "Coupled effect of variable Winkler–Pasternak foundations on bending behavior of FG plates exposed to several types of loading", *Steel Compos*. *Struct*., *Int*. *J*., **44**(3), 353-369. https://doi.org/10.12989/scs.2022.44.3.353

Irles-Más, R. and Irles-Más, F. (1992), "Alternativa analítica a la determinación de tensiones bajo zapatas rectangulares con flexión biaxial y despegue parcial", *Informes de la Construcción*, **44**(419), 77-89. https://dialnet.unirioja.es/servlet/articulo?codigo=2768804

Kaur, A. and Kumar, A. (2016), "Behavior of eccentrically inclined loaded footing resting on fiber reinforced soil", *Geomech*. *Eng*., *Int*. *J*., **10**(2), 155-174. https://doi.org/10.12989/gae.2016.10.2.155

Khajehzadeh, M., Taha, M.R. and Eslami, M. (2014), "Multi-objective optimization of foundation using global-local gravitational search algorithm", *Struct*. *Eng*. *Mech*., *Int*. *J*., **50**(3), 257-273. https://doi.org/10.12989/sem.2014.50.3.257

Lee, J., Jeong, S. and Lee, J.K. (2015), "3D analytical method for mat foundations considering coupled soil springs", *Geomech*. *Eng*., *Int*. *J*., **8**(6), 845-850. https://doi.org/10.12989/gae.2015.8.6.845

Lezgy-Nazargah, M., Mamazizi, A. and Khosravi, H. (2022), "Analysis of shallow footings rested on tensionless foundations using a mixed finite element model", *Struct*. *Eng*. *Mech*., *Int*. *J*., **81**(3), 379-394. https://doi.org/10.12989/sem.2022.81.3.379

López-Chavarría, S., Luévanos-Rojas, A. and Medina-Elizondo, M. (2017), "Optimal dimensioning for the corner combined footings", *Adv*. *Comput*. *Des*., *Int*. *J*., **2**(2), 107-121. https://doi.org/10.12989/acd.2017.2.2.169

López-Chavarría, S., Luévanos-Rojas, A., Medina-Elizondo, M., Sandoval-Rivas, R. and Velázquez-Santillán, F. (2019), "Optimal design for the reinforced concrete circular isolated footings", *Adv*. *Comput*. *Des*., *Int*. *J*., **4**(3), 273-294. https://doi.org/10.12989/acd.2019.4.3.273

Lu, X. and Aboutaha, R.S. (2021), "Strengthening of isolated square footings using passive wrapping systems", *Comput*. *Concrete*, *Int*. *J*., **27**(1), 41-54. https://doi.org/10.12989/cac.2021.27.1.041

Luévanos-Rojas, A. (2012a), "A mathematical model for dimensioning of footings square", *Int*. *Rev*. *Civil Eng*., **52**(4), 346-350.

Luévanos-Rojas, A. (2012b), "A mathematical model for the dimensioning of circular footings", *Far East J*. *Math*. *Sci*., **71**(2), 357-367.

Luévanos-Rojas, A. (2013), "A mathematical model for dimensioning of footings rectangular", *ICIC Express Letters*. *Part B*, *Applications: an International Journal of Research and Surveys*, **4**(2), 269-274.

Luévanos-Rojas, A. (2014), "Design of isolated footings of circular form using a new model", *Struct*. *Eng*. *Mech*., *Int*. *J*., **52**(4), 379-394. https://doi.org/10.12989/sem.2014.52.4.767

Luévanos-Rojas, A. (2015a), "A new mathematical model for dimensioning of the boundary trapezoidal combined footings", *Int*. *J*. *Innov*. *Comput*. *I*., **11**(4), 1269-1279. http://www.ijicic.org/ijicic-110411.pdf

Luévanos-Rojas, A. (2015b), "Design of boundary combined footings of trapezoidal form using a new model", *Struct*. *Eng*. *Mech*., *Int*. *J*., **56**(5), 745-765. https://doi.org/10.12989/sem.2015.56.5.745

Luévanos-Rojas, A. (2016), "A mathematical model for the dimensioning of combined footings of rectangular shape", *Rev*. *Tec*. *Fac*. *Ing*. *Univ*., **39**(1), 3-9. https://produccioncientificaluz.org/index.php/tecnica/article/view/21090/20946

Luévanos-Rojas, A. (2023a), "Optimization for trapezoidal combined footings: Optimal design", *Adv*. *Concrete Constr*., *Int*. *J*., **16**(1), 21-34. https://doi.org/10.12989/acc.2023.16.1.021

Luévanos-Rojas, A. (2023b), "New model for complete design of rectangular isolated footings taking into account that the contact surface works partially in compression", Revista ALCONPAT, **10**(3), 192-219. https://doi.org/10.21041/ra.v13i2.671

Luévanos-Rojas, A., López-Chavarría, S. and Medina-Elizondo, M. (2017). "Optimal design for rectangular isolated footings using the real soil pressure", *Ing*. *Invest*., **37**(2), 25-33. http://dx.doi.org/10.15446/ing.investig.v37n2.61447

Luévanos-Rojas, A., López-Chavarría, S. and Medina-Elizondo, M. (2018a), "A new model for T-shaped combined footings Part I: Optimal dimensioning", *Geomech*. *Eng*., *Int*. *J*., **14**(1), 51-60. https://doi.org/10.12989/gae.2018.14.1.051

Luévanos-Rojas, A., López-Chavarría, S. and Medina-Elizondo, M. (2018b), "A new model for T-shaped combined footings Part II: Mathematical model for design", *Geomech*. *Eng*., *Int*. *J*., **14**(1), 61-69. https://doi.org/10.12989/gae.2018.14.1.061

Luévanos-Rojas, A., Santiago-Hurtado, G., Moreno-Landeros, V.M., Olguin-Coca, F.J., López-León, L.D. and Diaz-Gurrola, E.R. (2024a), "Mathematical Modeling of the Optimal Cost for the Design of Strap Combined Footings", *Math*., **12**(2), 1-20. https://doi.org/10.3390/math12020294

Luévanos-Rojas, A., Moreno-Landeros, V.M., Santiago-Hurtado, G., Olguin-Coca, F.J., López-León, L.D., Baltazar-Zamora, M.A. and Diaz-Gurrola, E.R. (2024b), "Mathematical Modeling for the Optimal Cost Design of Circular Isolated Footings with Eccentric Column", *Math*., **12**(5), 1-19. https://doi.org/10.3390/math12050733

Luévanos-Soto, I., Luévanos-Rojas, A., Moreno-Landeros, V.M., Santiago-Hurtado, G. (2024a), "Minimum area for circular isolated footings with eccentric column taking into account that the surface in contact with the ground works partially in compression", *Couple*. *Syst*. *Mech*., *Int*. *J*., **13**(3), 201-217. https://doi.org/10.12989/csm.2024.13.3.201

Luévanos-Soto, I., Luévanos-Rojas, A., Moreno-Landeros, V.M., Santiago-Hurtado, G. (2024b), "Minimum cost design for circular isolated footings with eccentric column taking into account that the surface in contact with the ground works partially in compression", *Couple*. *Syst*. *Mech*., *Int*. *J*., **13**(4), 311-335. https://doi.org/10.12989/csm.2024.13.4.311

Mansour, W., Fayed, S. and Basha, A. (2022), "Experimental and numerical analysis of the punching behavior of RC isolated footings", *Steel Compos*. *Struct*., *Int*. *J*., **45**(5), 665-682. https://doi.org/10.12989/scs.2022.45.5.665

Montes-Paramo, P., Luevanos-Rojas, A., López-Chavarría, S., Medina-Elizondo, M. and Sandoval-Rivas, R. (2023), "Optimal area for rectangular combined footings assuming that the contact surface with the soil works partially to compression", *Ingeniería Investigación y Tecnología*, **24**(2), 1-15. https://doi.org/10.22201/fi.25940732e.2023.24.2.012

Özmen, G. (2011), "Determination of Base Stresses in Rectangular Footings under Biaxial Bending", *Teknik Dergi Digest*., **22**(4), 1519-1535. http://www.imo.org.tr/resimler/dosya_ekler/7b559795bd3f63b_ek.pdf?dergi=472

Peck, R.B., Hanson, W.E. and Thornburn, T.H. (1974), *Foundation Engineering*, (2nd Edition), John Willy & Sons, New York, NY, USA.

Rawat, S., Mittal, R.K. and Muthukumar, G. (2020), "Isolated rectangular footings under biaxial bending: a critical appraisal and simplified analysis methodology", *Pract*. *Period*. *Struct*. *Des*. *Constr*., **25**(3), p. 04020011. https://doi.org/10.1061/(ASCE)SC.1943-5576.0000471

Rodriguez-Gutierrez, J.A. and Aristizabal-Ochoa, J.D. (2013a), "Rigid spread footings resting on soil subjected to axial load and biaxial bending. I: Simplified analytical method", *Int*. *J*. *Geomech*., **13**(2), 109-119. https://doi.org/10.1061/(ASCE)GM.1943-5622.0000218

Rodriguez-Gutierrez, J.A. and Aristizabal-Ochoa, J.D. (2013b), "Rigid Spread Footings Resting on Soil Subjected to Axial Load and Biaxial Bending. II: Design Aids", *Int*. *J*. *Geomech*., **13**(2), 120-131. https://doi.org/10.1061/(ASCE)GM.1943-5622.0000210

Soto-García, S., Luévanos-Rojas, A., Barquero-Cabrero, J.D., López-Chavarría, S., Medina-Elizondo, M., Farias-Montemayor, O.M. and Martínez-Aguilar, C. (2022), "A New Model for the contact surface with soil of circular isolated footings considering that the contact surface works partially under compression", *Int*. *J*. *Innov*. *Comput*. *Inform*. *Control*, **18**(4), 1103-1116. http://www.ijicic.org/ijicic-180406.pdf

Teng, W.C. (1979), *Foundation Design*, Prentice-Hall Inc., New Delhi, India.

Turedi, Y., Emirler, B., Ornek, M. and Yildiz, A. (2019), "Determination of the bearing capacity of model ring footings: Experimental and numerical investigations", *Geomech*. *Eng*., *Int*. *J*., **18**(1), 29-39. https://doi.org/10.12989/gae.2019.18.1.029

Vela-Moreno, V.B., Luévanos-Rojas, A., López-Chavarría, S., Medina-Elizondo, M., Sandoval-Rivas, R. and Martinez-Aguilar, C. (2022), "Optimal area for rectangular isolated footings considering that contact surface works partially to compression", *Struct*. *Eng*. *Mech*., *Int*. *J*., **84**(4), 561-573. https://doi.org/10.12989/sem.2022.84.4.561

Velázquez-Santillán, F., Luévanos-Rojas, A., López-Chavarría, S., Medina-Elizondo, M. and Sandoval-Rivas, R. (2018), "Numerical experimentation for the optimal design for reinforced concrete rectangular combined footings", *Adv*. *Comput*. *Des*., *Int*. *J*., **3**(1), 49-69. https://doi.org/10.12989/acd.2018.3.1.049

Yáñez-Palafox, J.A., Luévanos-Rojas, A., López-Chavarría, S. and Medina-Elizondo, M. (2019), "Modeling for the strap combined footings Part II: Mathematical model for design", *Steel Compos*. *Struct*., *Int*. *J*., **30**(2), 109-121. https://doi.org/10.12989/scs.2019.30.2.109

Young, W.C. and Budynas, R.G. (2002), *Roark's Formulas for Stress and Strain*, (7th Edition), McGraw-Hill, NJ, USA.

CC